https://doi.org/10.5194/egusphere-2026-1303
Preprint. Discussion started: 26 March 2026

CoRSEER: The Calculator of Rock Surface Exposure Age and Erosion Rates for Rock Surface Luminescence dating

Arbaz N. Pathan[1]*, Rabiul H. Biswas[1], Devender Kumar[2,3]

[1] Department of Earth Sciences, Indian Institute of Technology Kanpur, Kanpur, 208016, India
[2] CSIR-National Geophysical Research Institute (NGRI), Uppal Road, Hyderabad, Telangana 500007, India
[3] Academy of Scientific and Innovative Research (AcSIR), Ghaziabad, Uttar Pradesh 201002, India

Correspondence to Arbaz N. Pathan (akp20@iitk.ac.in)

Abstract.

Rock-surface luminescence dating estimates the duration of rock surface exposure and the rate of erosion by analysing changes in luminescence with depth below the surface. The wider use of this method has been slowed by three practical issues: the subjective selection of the deep plateau for profile normalisation, inconsistent modelling choices across studies, and the lack of a unified inverse-modelling workflow that delivers both parameter estimates and uncertainty bounds. We introduce CoRSEER, an open-source MATLAB application that standardises the full workflow from luminescence depth profiles to exposure and erosion history. CoRSEER first normalises profiles objectively using weighted three-parameter logistic sigmoidal fitting to identify the saturation level and profile shape. It then simulates profile evolution with a finite-difference forward model that includes ambient radiation induced signal growth, depth-dependent bleaching described by a surface bleaching rate, attenuation coefficient, and advection caused by erosion. Finally, CoRSEER performs Monte Carlo inversion to estimate calibration parameters from known-age calibration samples, apparent exposure ages for unknown samples, and steady or stepwise erosion histories while reporting the best-fit and uncertainty ranges from likelihood-based filtering. We tested all three modules by reanalysing published datasets from multiple regions, including 23 calibration samples from the original dataset. For a representative calibration profile, CoRSEER improved the fit (coefficient of determination of 0.928 compared with 0.868 for the literature dataset) and substantially tightened the uncertainty bounds after objective re-normalisation. Across the compiled studies, the CoRSEER-derived apparent ages cluster close to the one-to-one line relative to the published values and span approximately 1–8.5 thousand years, while erosion estimates for a benchmark case remain comparable to the literature results (0.1 mm/a versus 0.066 mm/a). These results show that objective normalisation plus a transparent, standardised inversion framework can materially improve the reproducibility of rock surface luminescence dating and support consistent inter-study comparisons of exposure and erosion history.

Short Summary:

We developed CoRSEER, a user-friendly MATLAB based software that estimates the duration of rock surface exposure and the rate of erosion using the effect of sunlight on trapped electrons present below the surface. The program applies objective curve fitting, simulates how sunlight resets the signal and how erosion removes material, and reports uncertainties and fits them to an unknown data set. Tests on published datasets provide consistent results and better reproducibility, improving the reconstruction of past landscapes and climate change.

Keywords: Rock Surface Exposure Dating, Infrared Stimulated Luminescence, Rock surface exposure and erosion rate modelling, CoRSEER

https://doi.org/10.5194/egusphere-2026-1303
Preprint. Discussion started: 26 March 2026

1 Introduction

Reconstructing the timing of rock surface exposure and erosion history is crucial in geomorphology because it links climate, tectonics, and surface processes that shape the landforms observed today (Molnar and England, 1990). Generally, there are two major reconstruction scenarios. First, host rocks such as valley walls, bedrocks, or strath surfaces, and establishing the exposure ages of these surfaces can predict the age of the natural and anthropogenic events that remove the cover (e.g. deglaciation, stripping of the regolith, and quarrying), thereby beginning a new exposure clock (Owen and Dortch, 2014; Gliganic et al., 2019). Second, transportable clasts, such as cobbles and boulders, have transportation, deposition, and reworking histories that can be reconstructed if their exposure ages are known (Luo et al., 2018). However, establishing the erosion rates of these rock surfaces will provide information on the interactions between climate and landforms (Burbank et al., 1996). Evaluating the exposure-erosion history provides chronological and quantitative constraints on landscape evolution (Colman, 1981).

Terrestrial cosmogenic nuclide (TCN) dating has been extensively used to quantify rock surface exposure age and erosion rate (Lal, 1991; Balco et al., 2008; Schaefer et al., 2022; Dunai, 2010). ^{10}Be dating, the most commonly used technique, is sensitive only above the millennial timescale (Schaefer et al., 2022). Furthermore, the unique concentration of ^{10}Be can provide an infinite pair of exposure-erosion histories (Lehmann et al., 2019a) when the growth of ^{10}Be is in a transient state; lower exposure-lower erosion may have a similar effect as higher exposure–higher erosion. Thus, an independent chronometer and/or the use of an additional nuclide is required to constrain both the exposure and erosion histories. Furthermore, the choice of different scaling models has a high impact on the derived exposure ages, and because of the unavailability of a production rate calibration site in most geologically significant sites (e.g. the Himalayan-Tibetan orogen), this problem becomes more critical (Owen and Dortch, 2014).

The introduction of the novel RSLD has shown promising possibilities for overcoming some of these limitations and providing an additional independent chronometer. When rock is shielded from sunlight (part of the host rock or covered by opaque materials) and exposed to ambient radiation over Ma, the ionising radiation fills electron traps to field saturation in minerals such as quartz and feldspar (Wintle and Murray, 2006). When exposed to sunlight, it penetrates the rock surface, causing instantaneous detrapping of electrons, that is, bleaching of the luminescence signal on the surface. As the photon flux attenuates with depth, the bleaching rate decreases, causing a sigmoidal distribution of luminescence signals, also called the luminescence depth profile (LDP) (Sohbati et al., 2011; Sohbati et al., 2012a). The LDP is highly sensitive to exposure and erosion but weakly sensitive to ambient dose rates. While exposure causes deeper propagation of the LDP, erosion and ambient dose cause advection towards the surface (Sohbati et al., 2018; Lehmann et al., 2019a). Even exposure of <1 year can be significant enough to cause a sigmoidal distribution. Conversely, erosion at extremely low erosion rates (order of 10^{-5} mm/a) can cause measurable advection of the LDP (Pathan et al., 2024). We argue that the RSLD has the potential to act as a complementary method to TCN dating, and the RSLD-TCN coupled framework has been introduced in a few studies (Lehmann et al., 2019a; Smedley et al., 2021; Sohbati and Hippe, 2023). A comparison of TCN and RSLD dating is shown in Table 1.

Table 1: A comparison of TCN and RSLD

Comparative parameter	Terrestrial Cosmogenic Nuclides dating using ^{10}Be	Rock-surface Luminescence Dating
Signal principle	In-situ nuclide production in the top few meters by secondary cosmic rays; concentration accumulates with exposure and competes with decay and erosion.	Sunlight bleaches trapped charge in the outer few cm of rock; post-exposure, a depth-dependent luminescence profile develops whose shape reflects exposure time, erosion, and light penetration.
Exposure dating Range	Generally, from 10^3 to 10^6 years but is mainly affected by erosion. Lower rate of erosion (< 10^{-4} mm/a) will have no effect, but higher rate of erosion (>10^{-2} mm/a) can significantly reduce the maximum dateable age (Lal, 1991).	The minimum dateable age is ~1 year (often months) given adequate light, and the maximum dateable age is around 50 kyr to 100kyr, which is highly sensitive to even lower erosion rate on the order of 10^{-4} mm/a, causing a reduction in maximum dateable age (Pathan et al., 2024).

https://doi.org/10.5194/egusphere-2026-1303
Preprint. Discussion started: 26 March 2026

Calibration	Requires production-rate calibration and scaling to site conditions (Schaefer et al., 2022). Location and sample specific calibration is difficult and generally not performed.	Requires calibration of optical bleaching kinetic parameters (i.e., $\overline{\sigma\varphi_0}$, μ) to site conditions (Sohbati et al., 2012a). It is easier to do location and specific calibration.
Scaling/model dependence	Multiple scaling schemes for estimating production rates, such as Lal/Stone (Stone, 2000), the Dunai Scaling model (Dunai, 2000), the Lifton-Sato-Dunai (LSD) model (Lifton et al., 2014), Desilets and Zreda model (Desilets and Zreda, 2003), are available. Predicted exposure age greatly affected by the choice of model S(Owen and Dortch, 2014; Schaefer et al., 2022).	Various RSLD models are available, such as the first-order kinetic model (FOK) (Sohbati et al., 2012b), fading model (Freiesleben et al., 2023; Jain et al., 2015) and general order kinetic model (GOK) (Freiesleben et al., 2023a, Biswas et al., 2023, Pathan et al., 2024). The derived exposure-erosion history highly depends on the choice of models and the superiority of GOK model is established though (Pathan et al., 2024).
Advantages	Robust for multi-kyr exposures; simple sampling; extensive literature; pairing of nuclides provides erosion information.	Resolves short exposures; broad erosion-rate sensitivity; field calibration is logistically straightforward.
Limitations	Weak for decadal–centennial exposures; high erosion biases ages; inheritance can over-age clasts; scaling/PR uncertainties; cost/AMS access (Owen & Dortch, 2014; Schaefer et al., 2022).	Strong dependence on modelling aspect and derived calibration parameters; higher uncertainty in higher exposure ages; different kinetics model for feldspar IRSL; community-standard codes/workflows still emerging .
Best suited materials/settings	Quartz-bearing lithologies; stable bedrock; moraines/erosional surfaces with low–moderate erosion (Schaefer et al., 2022).	Feldspar and/or quartz-bearing rocks with light-exposed surfaces; settings with recent exposure or erosion (e.g., deglaciated bedrock, rockfall blocks, anthropogenic cuts).

2 Model

The choice of the incorporated model significantly affects the chronology derived using the RSLD. Thus, it is crucial to include the most accurate, peer-reviewed, simple, and flexible model that can encompass all the geological scenarios for the most robust chronology. This section reviews the RSLD models and discusses which one we choose as the most accurate.

Table 2: Symbology, units, and descriptions of parameters used.

n	*number unit*	Number of trapped electrons
N		Maximum possible number of trapped electrons
$\bar{n}$	*dimensionless*	Normalised electron trap population
$\bar{n}_{sim}$		Simulated normalised luminescence signal
$\bar{n}_{obs}$		Natural normalised luminescence signal
σ	mm^2	Luminescence photoionisation cross section
φ_o	$mm^{-2}.s^{-1}$	Photon flux on the surface of the rock
$\overline{\sigma\varphi_0}$	s^{-1}	Wavelength-dependent decay constant of rocks
μ	mm^{-1}	Attenuation coefficient
$\dot{D}$	$Gy.a^{-1}$	Environmental dose rate
D_o	Gy	Characteristic dose of saturation (Dose that fills ~63% of the traps (Wintle and Murray, 2006)
r	*dimensionless*	Order of Kinetics (Biswas et al., 2023; Freiesleben et al., 2023)
L_x	$counts.s^{-1}$	The luminescence intensity of the natural sample
T_x	$counts.s^{-1}$	The luminescence intensity of the laboratory-dosed sample
L_x/T_x	*dimensionless*	The laboratory-dose normalised luminescence intensity for the natural sample
a	*dimensionless parameters of Eq. 16*	upper asymptote, the maximum value the function can attain when $x \sim \infty$
b		steepness of the curve or growth rate of the curve
c		depth of the inflection point, also referred to as $x_{0.5}$
χ^2	*dimensionless*	*Chi-square*
P_k		Likelihood value associated with the synthetic LDP numbered as k

https://doi.org/10.5194/egusphere-2026-1303
Preprint. Discussion started: 26 March 2026

P_{max}		Maximum likelihood, which is associated with the best-fitting synthetic LDP
P^{k}_{norm}		Normalised likelihood value associated with the synthetic LDP numbered as k
δ		Standard deviation
α		fractional error, which is equal to $(Lx/Tx)/(Lx/Tx)_{error}$
R^2		Coefficient of determination
x	*mm*	Depth from surface
$x_{0.5}$		Depth of Half Saturation from the surface
$x_{0.5,max}$		Forward modelled half saturation depth associated with maximum detectable age limit.
$x_{0.5,ss}$		Forward-modelled half-saturation depth when the LDP is in a steady state and purely acts as an erosion meter
$x_{0.5,natural}$		Half saturation depth for natural LDP also equals the c value
t	*a*	Exposure age
t_{max}		Maximum age limit for the samples
t_i		Independent exposure age by any other method
t_{cal}		Known exposure age of calibration sample
t_s		Onset time of erosion
t_{ss}		Steady-state erosion time
$\dot{\varepsilon}$	*mm/a*	Erosion rate
$\dot{\varepsilon}_{ss}$		Steady-state erosion rates

2.1 Laskaris and Liritzis. (2011)

This is the first parametric fit function presented for rock-surface luminescence dating (Laskaris and Liritzis, 2011). This was suggested for both OSL and TL.

$$(x; a_1, b_1, c_1, d_1) = a_1 + \frac{b_1}{2}\, erfc\left(\frac{\ln\left(\frac{x}{c_1}\right)}{d_1\sqrt{2}}\right) \quad (1)$$

where L is distribution of luminescence signal with respect to depth and its dependent on the fitting parameters as $a_1, b_1, c_1, and\ d_1$. While this empirical model enables precise fitting to the luminescence depth profile, it does not explain the luminescence mechanism inside the rock, and the derived fitting parameters are not linked to the natural kinetic parameters. Additionally, this model assumes zero erosion conditions, which are not always achievable. Thus, this model was not incorporated into any further RSLD studies.

2.2 Sohbati et al. (2018)

Sohbati et al. (2018) proposed a model whereby the instantaneous concentration of trapped electrons n at depth x is:

$$\frac{dn}{dt} = (N - n)F(x) - nE(x) \quad (2)$$

where,

$$E(x) = \overline{\sigma\varphi_0}\mathrm{e}^{-\mu x} \quad (3)$$

$$F = \dot{D}(x)/D_0 \quad (4)$$

With the boundary conditions $n = N$ at $t = 0$, the analytical solution was evaluated as

$$\frac{n(x,t)}{N} = \frac{E(x)e^{-t[E(x)+F]} + F}{E(x) + F} \quad (5)$$

https://doi.org/10.5194/egusphere-2026-1303
Preprint. Discussion started: 26 March 2026

$$\frac{n(x,t)}{N} = \frac{\overline{\sigma\varphi_0}e^{-\mu x}e^{-t\left(\overline{\sigma\varphi_0}e^{-\mu x}+\frac{\dot{D}}{D_0}\right)} + \frac{\dot{D}}{D_0}}{\overline{\sigma\varphi_0}e^{-\mu x} + \frac{\dot{D}}{D_0}} \quad (6)$$

The model was further improved by incorporating an erosion scenario (Sohbati et al., 2018).

$$x(t) = x_0 - \dot{\varepsilon}t \quad (7)$$

$$E\big(x(t)\big) = \overline{\sigma\varphi_0}e^{-\mu(x_0-\dot{\varepsilon}t)} = (\overline{\sigma\varphi_0}e^{-\mu x_0})e^{\mu\dot{\varepsilon}t} = E_0e^{\mu\dot{\varepsilon}t} \quad (8)$$

$$\frac{dn}{dt} = (N-n)F - nE_0e^{\mu\dot{\varepsilon}t} \quad (9)$$

Where,

The analytical solution as a confluent hypergeometric function is

$$\frac{n(x,\dot{\varepsilon})}{N} = M\left(1{,}1 + \frac{F}{\mu\dot{\varepsilon}}, -\frac{E(x)}{\mu\dot{\varepsilon}}\right) \quad (10)$$

The analytical solution improves the feasibility of modelling by incorporating the effects of dose rates, FOK decay behaviour and erosion. However, this model is far from accurate in the case of polymineral or feldspar samples, where the infrared stimulated luminescence (IRSL) of feldspar minerals exhibits non-first-order decay; thus, the GOK model is applicable to these samples.

2.3 Freiesleben et al. (2023) Model

Freiesleben et al. (2023) developed this model to incorporate GOK:

$$\frac{dn}{dt} = -E_{\dot{\varepsilon}}(x,t)n^r \quad (11)$$

where r = order of kinetics

$$E_{\dot{\varepsilon}}(x,t) = \overline{\sigma\varphi_0}e^{-\mu(x_0-\dot{\varepsilon}t)} \quad (12)$$

$$n(x,t_{\dot{\varepsilon}}) = [(b-1)t_{\dot{\varepsilon}}E(x) + n^{1-r}]^{\frac{1}{1-r}} \quad (13)$$

where the apparent exposure time is given as

$$t_\varepsilon = \frac{1}{\mu\dot{\varepsilon}}\left(1 - e^{-\mu\dot{\varepsilon}t}\right) \quad (14)$$

This model considers the order of kinetics and erosion scenario but ignores the effect of the dose rate on LDP) propagation. However, in natural environments, the dose rate considerably affects the propagation of LDP over a longer timescale (>10^3 years), and this effect is amplified with an increase in the order of kinetics (Pathan et al., 2024). This model also assumes a constant average rate of erosion, which may not be applicable in different erosion scenarios, such as step-function or stochastic histories (Ganti et al., 2016; Brown and Moon, 2019; Lehmann et al., 2019a).

2.4 Model Framework after Biswas et al. (2023), Lehman et al. (2019a), Pathan et al. (2024)

$$\frac{d\overline{n}}{dt} = \left\{\frac{\dot{D}}{D_o}(1-\overline{n})\right\}_{growth} - \left\{\overline{n}^r\,\overline{\sigma\varphi}_\circ e^{-\mu x}\right\}_{decay} + \left\{\dot{\varepsilon}\frac{d\overline{n}}{dx}\right\}_{erosion} \quad (15)$$

The modelling framework adopted in this study (Eq. Model (15) brings together key components that earlier models did not include: (1) near-realistic representation of the luminescence mechanism, (2) general order kinetics, (3) erosion incorporation with a natural mechanism, and (4) dose rate effect. This was required to accurately simulate the luminescence signal evolution on rock surfaces and was built upon earlier work (Lehmann et al., 2019; Biswas et al., 2023; Pathan et al., 2024). The model incorporates signal accumulation through the environmental dose (growth), flux, and wavelength-dependent decay, including the nonlinear decay of the IRSL and advective loss due to erosion. Thus, a realistic simulation of the LDP was achieved. This model has been successfully used in several studies. Lehmann et al. (2019) and Elkadi et al. (2022) used this model assuming FOK (r = 1) to jointly invert ^{10}Be cosmogenic nuclide data and RSLD profiles, enabling robust estimation of erosion histories and erosion corrected exposure age

https://doi.org/10.5194/egusphere-2026-1303
Preprint. Discussion started: 26 March 2026

through complementary dating systems. Smedley et al. (2021), Brill et al. (2021), and others applied this model to reconstruct complex erosion histories, also assuming FOK. Furthermore, Biswas et al. (2023) and Pathan et al. (2024) improved this model by incorporating General Order Kinetics (GOK). This enhancement significantly increased the model's applicability, particularly for feldspar-based IRSL signals, where slower decay (than predicted from the FOK model) behaviour is commonly observed. The FOK model assumes a simple exponential decay, with *r* equal to 1, while the GOK model introduces a shape parameter r that captures the slower, non-exponential bleaching behaviour observed in feldspar signals (Duller, 1997; Chen and Leung, 2003; Guralnik et al., 2015). This refinement led to more accurate estimates of exposure duration and erosion rates. Studies have shown that using the FOK model may generally result in overestimating erosion rates and underestimating exposure ages by up to an order of magnitude (Biswas et al., 2023; Pathan et al., 2024; Luo et al., 2026). By embedding this comprehensive model into the CoRSEER platform, we attempt to provide users with a powerful and reproducible toolset for forward-inverse modelling, leading to robust exposure–erosion history reconstruction.

3 Methodology

CoRSEER is a MATLAB-based app designed to streamline the quantification of rock-surface exposure age (for uneroded surfaces) and erosion histories (for eroded surfaces) through inverse modelling of luminescence depth profiles. The workflows are as follows.

3.1 Normalisation of experimental data

To eliminate the effect of intersample variability (mass and luminescence production efficiency), the test-dosed normalised luminescence (L_x/T_x) was measured at different depths to generate the LDP. The LDP is further adjusted (or normalised) to plateau at 1 to facilitate further mathematical operations (Sohbati et al., 2012a). Traditionally, users select a depth beyond which the experimental LDP is assumed to be saturated through visual inspection and compute the mean L_x/T_x of all points thereafter to normalise the entire profile. However, the high scatter in the saturation region often leads to subjective depth selection, introducing human error and bias. The incorrectly identified plateau can systematically distort the normalised signals and skew the kinetic parameter estimation. To overcome this, we present an empirical normalisation using the sigmoidal curve fitting (SCF) method. We chose the following three-parameter logistic sigmoidal function (Kaufmann, 1981) to model the luminescence-depth profile:

$$f(x) = \frac{a}{1 + exp[-b(x - c)]} \tag{16}$$

where a is the upper asymptote, the maximum value the function can attain as $x \sim \infty$, denotes the saturation luminescence intensity (or L_x/T_x), *and b* is the growth rate, which controls the steepness of the curve. A higher *b* indicates a steeper transition of L_x/T_x with depth. *c* represents the inflection point or $x_{0.5}$, that is, the depth at which half of the saturation signal is reached (Fig. 1). To derive *a*, *b*, and *c*, we fitted Eq. 16 with experimental LDP using weighted nonlinear least-squares regression fitting using MATLAB fit curve. The initial guesses for fitting parameters were set to $a_0 = max\left(\frac{L_x}{T_x}\right)$, $b_0 = 1$ and $c_0 = median(x)$. We enforced bounds to ensure physically meaningful solutions:(a) Lower bounds: [0, 0, 0](b) Upper bounds: [∞, ∞, *max(x)*] and provide the weight factors (w_i) as $w_i = \frac{1}{\alpha}$ where α is the fractional error. The experimentally observed LDP (L_x/T_x vs. depth) was normalised with the respective *a* value for each sample and termed as SCF-normalised LDP. This approach was used to identify the plateau and normalise the experimental data. This method removes bias, improves reproducibility, and ensures a consistent LDP normalisation algorithm across diverse datasets by eliminating manual intervention.

https://doi.org/10.5194/egusphere-2026-1303
Preprint. Discussion started: 26 March 2026

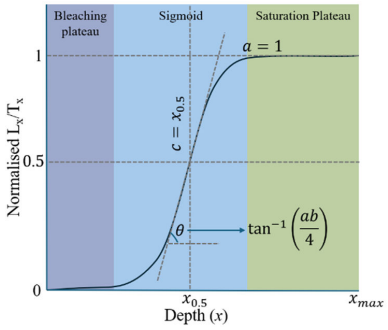

Figure 1: The luminescence-depth profile (LDP) sigmoidal shape consists of three distinct regions: 1) the near-surface bleaching plateau, 2) the middle slope ($tan\,\theta = \left(\frac{ab}{4}\right)$ at $c = x_{0.5}$) of sigmoidal shape, and 3) the deep saturation plateau of magnitude 'a'.

3.2 Inverse Modelling in CoRSEER

In inverse modelling, multiple LDPs are simulated by solving Eq. 15 using finite difference method for two main scenario as: (a) varying kinetic parameters, $\overline{\sigma\varphi_0}$, and μ (keeping the exposure-erosion history as fixed) or (b) by varying the exposure-erosion history (keeping $\overline{\sigma\varphi_0}$, and μ as fixed). For calibration sample (known exposure-erosion history), kinetic parameters ($\overline{\sigma\varphi_0}$, and μ) are randomly varied whereas for natural samples (known $\overline{\sigma\varphi_0}$, and μ), exposure-erosion history is randomly varied. The other kinetic parameters, $\dot{D}$, D_o, and r are constrained independently using DRAC (Durcan et al., 2015; Sohbati et al., 2018), IRSL dose-response curve (Wintle and Murray, 2006) and fitting decay of IRSL with light exposure (Biswas et al., 2023) respectively. These parameters are user-defined in CoRSEER. Out of multiple LDPs, most probabilistic LDPs or best fitted LDP and corresponding parameters are constrained by comparing the simulated LDPs ($\bar{n}_{sim}$) and experimentally observed SCF normalised LDP ($\bar{n}_{obs}$) and by minimising the misfit, using metrics like chi-square (χ^2) and maximising the *likelihood,* following the approach by Lehmann et al. (2019a).

$$\chi^2 = \sum_{i=1}^{l} \frac{\left((\bar{n})_{obs}^{(i)} - (\bar{n})_{sim}^{(i)}\right)^2}{\sigma^2} \quad (17)$$

$$likelihood = P = e^{-\chi^2/2} \quad (18)$$

$$P_{norm}^{k} = \frac{P_k}{P_{max}} \quad (19)$$

where l is the number of experimental data points, δ is the standard deviation of the residual between observed profile and best-fitting SCF profile divided by a factor, P_k is likelihood value associated with simulated LDP numbered as k, P_{max} is maximum-likelihood which associates with best-fitting synthetic LDP and P_{norm}^{k} is normalised likelihood value associated with simulated LDP numbered as k. The best LDP and corresponding parameters were selected by applying the Monte-Carlo acceptance criterion as $P_{norm}^{k} > R$, where R is a random number between zero and one. Finally, CoRSEER establishes the values of best-fit, median, ±1δ,and ±2δ for all required parameters with confidence intervals.

3.2.1 Calibration

CoRSEER I module constrain $\overline{\sigma\varphi_0}$ and μ from SCF normalised LDP of calibration sample (known exposure age and known erosion rate). The inverse modelling (described above) is performed with fixed input parameters are, $\dot{D}$, D_o, r, t and $\dot{\varepsilon}$ and random selection of $\overline{\sigma\varphi_0}$ and μ from user defined range for a large number of iterations. It must be mentioned that erosion is assumed to be negligible

https://doi.org/10.5194/egusphere-2026-1303
Preprint. Discussion started: 26 March 2026

for the young calibration sample. However, for the older calibration sample, erosion might not be zero which may bias the parameter estimates. The CoRSEER I – Calibration has option to include erosion rate ($\dot{\varepsilon} > 0$), if known.

The parameter pair ($\overline{\sigma\varphi_0}$ and μ) associated with the lowest normalised chi-square is designated the best-fit bleaching parameter. To assess uncertainty, CoRSEER-I filters the entire chi-square field using a probabilistic threshold: all solutions where $P_{norm}^{k} > \text{rand}(m, m)$ (following the method of Pathan et al. 2024) are retained, and their median and 1-sigma uncertainty bounds are reported. This approach ensures the statistical robustness and physical interpretability of the calibrated parameters. The details of the input, mechanism, and output of CoRSEER-I are discussed in Supplementary Section S3. These, location and rock type specific, calibration parameters ($\overline{\sigma\varphi_0}$ and μ) are used as inputs in exposure age and erosion rate calculation.

A representative analysis was performed on the LDP of the available literature data ROAD02 (Smedley et al., 2021). As we are solving for only one LDP corresponding to the IRSL50 signal, henceforth, the LDP is termed IR50_ROAD02. The LDP was normalised (the maximum value of Lx/Tx was set to 1) manually. This road-cut sample has an exposure age of 57 a (when the LDP was generated). The other parameters are $r = 1$, $\dot{D} = 4.76 \pm 0.15\ Gy/kyr$, and $D_o = 500\ Gy$. The inverse modelling is performed for 500 × 500 pairs of $\overline{\sigma\varphi_0}$ (ranging from 10^{-10} to 10^{0}, spacing in log-scale) and μ (ranging from 0 to 4) and considering no erosion. After the calibration is completed, CoRSEER generates three diagnostic plots, as shown in Fig. 2a-c.

The normalisation factor in the SCF analysis was estimated as a = 1.085 (Fig. 2a) which shows the presence of inaccurate normalisation due to human error, and the profiles were further renormalised (SCF normalisation) using this factor for accuracy. Fig. 2b-c shows the plausible fitting using CoRSEER-I comparable to fitting seen literature (Fig. 6g of Smedley et al. 2021). The resulting best-fitting $\overline{\sigma\varphi_0}$ and μ values are 1×10^{-7} s^{-1} and 1.08 mm^{-1} which vary significantly from reported values of 6.67×10^{-6} s^{-1} (overestimated by order of ~2) and 2.1 mm^{-1} (overestimated by factor of ~2) by Smedley et al. (2021). Furthermore the ±1δ range for $\overline{\sigma\varphi_0}$ is reduced from $1.27 \times 10^{-4} – 3.50 \times 10^{-7}$ s^{-1} to 6.39×10^{-8} - 3.11×10^{-7} s^{-1} and μ is reduced from 1.4 – 2.6 to 1.00 to 1.31 mm^{-1} showing the tightening of error width. We investigated the reason for this discrepancy between the results by comparing the manually normalised LDP (literature) from the SCF-normalised LDP (factor a = 1.085). We plotted the simulated profiles using the calibration dataset associated with both LDP (literature and CoRSEER-I, respectively). Fig. 2d shows that there is no tangible depth difference between the literature and CoRSEER-I generated profiles, but we see a noticeable difference in the slope of the LDPs. The estimated R^2 values were 0.868 for the literature dataset and 0.928 for CoRSEER-I, indicating greater precision in fitting with CoRSEER, as shown in Fig. 2e.

Despite the slight difference in the R^2 values, the evaluated kinetic parameters varied significantly. The apparent reason for this discrepancy might be caused by 1) SCF normalisation of the LDP and 2) the Fitting Strategy.

https://doi.org/10.5194/egusphere-2026-1303
Preprint. Discussion started: 26 March 2026

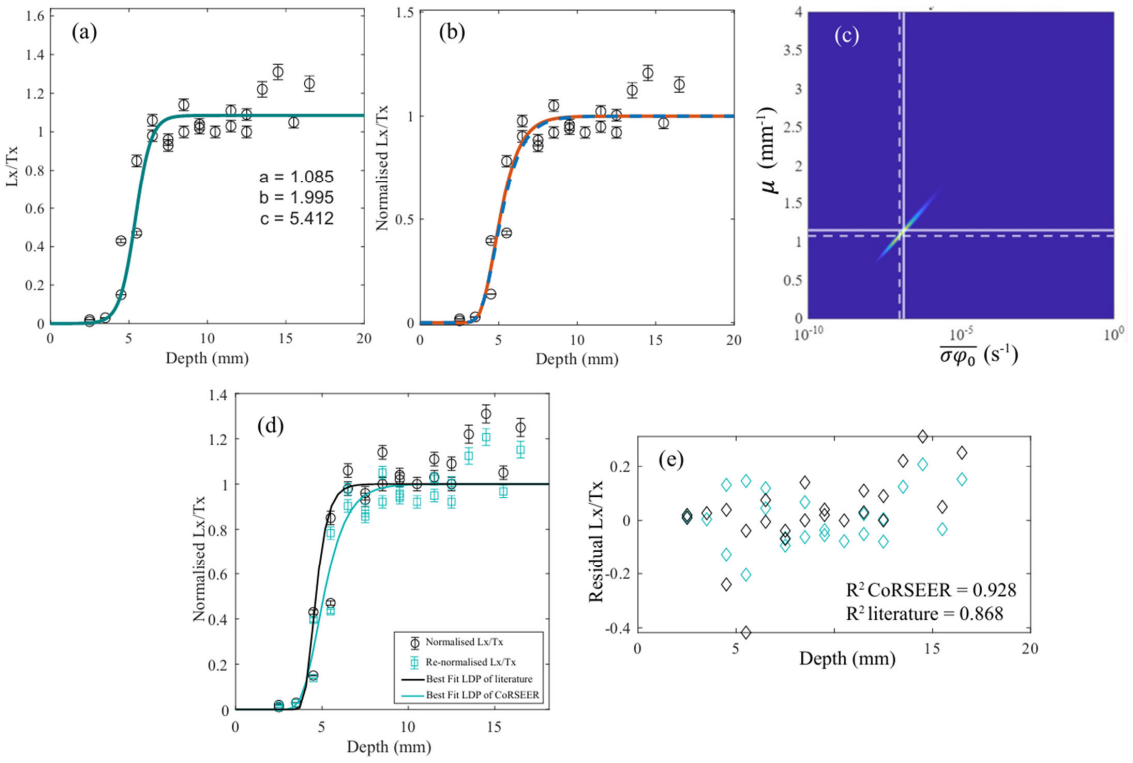

Figure 2: Re-evaluation of the IR50 calibration parameters for sample ROAD02 (IR50_ROAD02) (Smedley et al., 2021). (a) The natural IR50 L_x/T_x depth profiles (hollow circles) and associated sigmoidal fit (teal solid line). Although the normalisation was already performed by the Smedley et al. (2021), the fitted amplitude showed a = 1.085, indicating ~8.5% under-normalisation. Parameters b and c indicate the steepness and $x_{0.5}$, respectively. (b) The simulated LDPs for best-fit (dashed blue) and median (solid orange) calibration parameters associated with the SCF-normalised LDP (hollow circles). The precise overlap between both simulated LDPs shows a great agreement between the best-fit and median values indicating plausible fitting strategies. (c) Probability likelihood distribution in $\overline{\sigma\varphi_0}$ and μ space from Bayesian inversion. The dashed lines represent the best-fitting values, and the solid line represents the median of the filtered values using the criteria described in Section 3.2.2. (d) Direct comparison of the literature-normalised profile (black circles) and CoRSEER-ISCF-normalised profile (cyan square) alongside their corresponding best-fit simulated luminescence depth profile (black and cyan lines). Both datasets show comparative $x_{0.5}$, but there is a slight change in the slope after renormalisation. (e) Residuals (data − model) as a function of depth for both fits, highlighting the improved agreement for CoRSEER-I. The coefficient of determination increases from $R^2 = 0.868$ (literature handling) to $R^2 = 0.928$ (CoRSEER-I), indicating a tighter, more precise fit to the same underlying measurements.

3.2.2 Age Estimation

This module evaluates the exposure age from the LDP of an unknown sample for a no-erosion scenario. If the sample had an erosion history, the derived age would be the apparent exposure age (t_{app}). The inverse modelling is performed with fixed input parameters, $\dot{D}$, D_o, r, $\overline{\sigma\varphi_0}$, μ and $\dot{\varepsilon}$ and random selection of t from user defined range for a large number of iterations . A probabilistic threshold filter is applied (e.g., P^k_{norm} > rand(m, 1)) to extract accepted LDPs from which the best-fitting age, median age and $\pm 1\delta$ age uncertainty are derived. The algorithm also calculates t_{max}, the maximum possible exposure age which is associated with depth beyond which the LDP does not hold any information exposure history (x_{max}). Here, we define $x_{max} = x_{ss} - 1/\mu$, as described by Sohbati et al. (2018). We simulated the evolution of $x_{0.5}$, the depth at which the luminescence signal reaches 50% of the saturation signal. The simulation continued until $x_{0.5}$ asymptotically approached a steady-state depth *of* x_{ss}. The input, mechanism, and output of CoRSEER-II are discussed in Supplementary Section S4.

Here, we evaluated the exposure age of the avalanche boulder BALL02 (Smedley et al., 2021) (here termed as IR50_BALL02) using CoRSEER-II. The boulder was deposited and exposed due to an avalanche event dated as (*ti*) 4.52 ± 0.27 ka. Smedley et al. (2021) estimated the erosion uncorrected exposure of age (t_{app}) as 8 ± 2 a, which was evaluated using $\dot{D} = 3.32 \pm 0.12\ Gy/ka$,

https://doi.org/10.5194/egusphere-2026-1303
Preprint. Discussion started: 26 March 2026

D_o = 500 Gy, $\overline{\sigma\varphi_0}$ = 6.67 × 10^{-6} s^{-1}, μ = 2.1 mm^{-1}, $\dot{\varepsilon} = 0$ and r = 1 (The calibration parameters were evaluated from ROAD02). Here, we replace the calibration parameters, $\overline{\sigma\varphi_0}$, and μ with the values obtained in CoRSEER-I, $\overline{\sigma\varphi_0}$ = 1 × 10^{-7} s^{-1}, μ = 1.08 mm^{-1}, and keeping the other parameters ($\dot{D}$, D_o, r) same. CoRSEER-II generates three diagnostic plots, as shown in Fig. 3a-c.

The a = 1.032 shows (Fig. 3a) the presence of mild inaccurate normalisation, and unknown age LDP was renormalised. The impressive fitting of the SCF-normalised LDP with the accepted paths shows a successful inversion, as shown in Fig. 3b. The apparent exposure age calculated as 9 ± 1 a using CoRSEER-II is comparable to 8 ± 2 a as derived by Smedley et al. (2021). Despite the significant difference in calibration parameters derived from CoRSEER-I and the literature, we observed almost the same ages. This can be explained by the fact that the while performing single calibration (Sohbati et al., 2012b), the $\overline{\sigma\varphi}_\circ$ and μ can covary (Fig. 5c) and based on fitting strategies these both parameters can change. The calibration profile of higher log($\overline{\sigma\varphi}_\circ$) and μ will overlap to lower log($\overline{\sigma\varphi}_\circ$) and μ for the same age sample but the magnitude of slope of the sigmoid will be lesser for lower μ (Sohbati et al., 2018). Finally, this is affected by the precision of the model and fitting strategy used to account for the slope of the curvature.

Using the kinetic parameters given earlier, we simulate the propagation of the LDP through tracking the $x_{0.5}$ with a simulated exposure time (> 10^5) for different constant erosion rate scenarios ($\dot{\varepsilon}$ = 10^{-4}, 10^{-3}, 10^{-2}, 10^{-1}, 10^0, 0 mm/a), as shown in Fig. 3c. We plot two points on the no erosion $x_{0.5}$ line: i) The $x_{0.5,natural}$ (blue filled circle in Fig 3c) corresponds to the apparent exposure age. ii) x_{max} (red filled circle in Fig 3c), depth of maximum exposure age ($x_{max} < x_{ss} - 1/\mu$) . Thus, for a no-erosion scenario, the current sample can be dated up to an age of ~ 52 ka which is far higher than the actual exposure age (4.52 ± 0.27 ka) of the boulder. The highly underestimated apparent exposure age of 9 ± 1 a indicates that this sample underwent significant erosion. Assuming that the LDP is in a steady-state equilibrium, for current $x_{0.5,natural,}$ the erosion rates may lie between 10^{-2} and 10^0 mm/a. This represents the plausible performance and application of CoRSEER-II to derive and diagnose the apparent exposure ages and provide insight into the possible erosion rate.

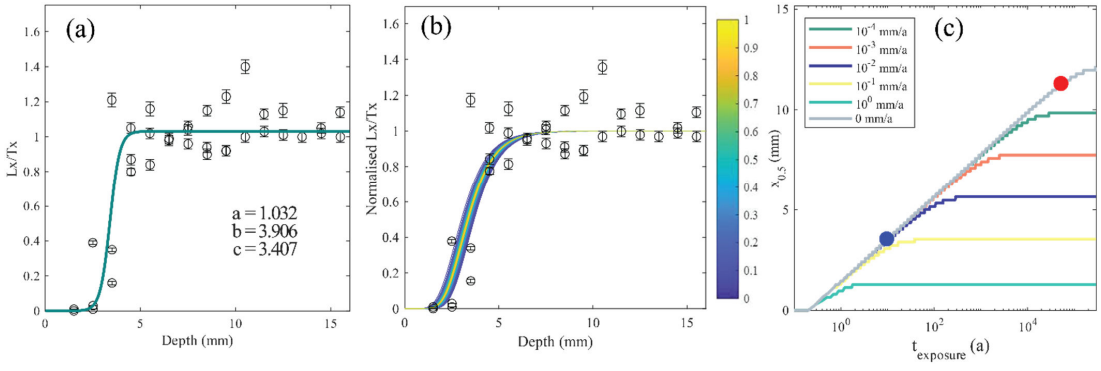

Figure 3: CoRSEER-II exposure-age inversion and erosion-diagnostic modelling for avalanche boulder IR50_BALL02. Unknown natural IR50 Lx/Tx depth profiles (hollow circles) and their sigmoidal fit (teal solid line). The fitted a = 1.032 shows 3.2% under normalisation, which was further used for SCF normalisation of the natural LDP. The *b*-value of 3.906 indicates a very steep slope.(b) The renormalised LDP (black hollow circles) and its corresponding Bayesian inversion fit resulting in the probability likelihood patch of ± δ exposure age LDP. Convergence towards the centre indicates an excellent fit to the model.(c) The evolution of $x_{0.5}$ for long-term exposure and constant erosion-rate (0, 10^{-4}, 10^{-3}, 10^{-2}, 10^{-1}, 10^0, mm/a) scenarios using $\dot{D} = 3.32 \pm 0.12$ Gy/kyr, D_o = 500 Gy, $\overline{\sigma\varphi_0}$ = 1 × 10-7 s-1, μ = 1.08 mm-1 and r = 1. The blue-filled circle denotes the $x_{0.5,\ natural}$, taken as the c value of the current profile from panel (a). The red-filled marker plotted on the zero-erosion $x_{0.5}$ line indicates the no-erosion chronometer limit ($x_{max} < x_{ss} - 1/\mu$), showing that the profile could, in principle, record ages up to ~52 ka if no ongoing erosion of the surface occurred.

3.2.3 Erosion Estimation:

Here, we evaluated the erosion history of a rock surface undergoing step-function erosion. Although the natural erosion pattern is more stochastic, we prefer the step-function history for computational simplicity, as used in previous studies (Smedley et al., 2021; Lehmann et al., 2019a; Lehmann et al., 2019b; Elkadi et al., 2022; Pathan et al., 2024). Using user-provided logarithmic spacing of exposure-erosion history, the CoRSEER-III creates two vectors: erosion rates ($\dot{\varepsilon}$) and exposure durations (t). If the erosion-corrected

https://doi.org/10.5194/egusphere-2026-1303
Preprint. Discussion started: 26 March 2026

exposure age is known by any other independent method, the t can be replaced with its value. For each ($\dot{\varepsilon}$, t) pair, it simulates LDPs using a two-phase approach: Phase 1 with no erosion (from 0 to purely exposure period (t_o)), and Phase 2 with constant erosion, $\dot{\varepsilon}$ (for the period of t_s) ($t = t_o + t_s$, total exposure age). This forward modelling solves Equation (15) using the finite difference method and produces the final simulated LDPs. We plot $\dot{\varepsilon}$-t_s matrix and its associated P^k_{norm} and interpret the exposure-erosion conditions. The input, mechanism, and output of CoRSEER-III are discussed in Supplementary Section S4.

We evaluated the exposure-erosion history of IR50_BALL02, which was suspected to face significant erosion, as discussed in Section 3.2.2. Smedley et al. (2021) estimated the steady-state erosion rate ($\dot{\varepsilon}_{ss}$) and erosion onset exposure age (t_{ss}) as 0.066 mm/a and 73 a, which was evaluated using $\dot{D} = 3.32 \pm 0.12\ Gy/kyr$, $D_o = 500\ Gy$, $\overline{\sigma\varphi_0}$ = 6.67 × 10^{-6} s^{-1}, μ = 2.1 mm^{-1}. If the t_{app} of a sample is much lower than the expected age (as observed for IR50_BALL02), the LDP is in a steady state due to exposure-erosion, and the maximum exposure age can be t_{max} (here 52 ka) for no erosion and model should be run for exposure duration of t_{max} if the exact exposure history is not known. As the boulder was previously dated to 4.52 ± 0.27 ka, we solved Eq. 15 for t of 5 ka (t_s value varied from 0 to 5 ka in log-scale) and the erosion rate range as 10^{-6} to 10^{1} mm/a (spacing in log-scale) as a 50 × 50 matrix using $\dot{D} = 3.32 \pm 0.12\ Gy/kyr$, $D_o = 500\ Gy$, $\overline{\sigma\varphi_0}$ = 1 × 10^{-7} s^{-1}, μ = 1.08 mm^{-1} and r = 1. After completion, the CoRSEER-III generates the two diagnostic plots: (1) Sigmoidal fitting (already shown in Fig. 3a), (2) the probability likelihood surface plot of $\dot{\varepsilon}$-t_s pairs as shown in Fig. 4. We derive the $\dot{\varepsilon}_{ss}$ as 0.1 mm/a and t_{ss} as 88 a using CoRSEER-III, which is comparable to the rate 0.066 mm/a and 73 a as shown in Fig. 4. This established the applicability of CoRSEER-III for predicting erosion rates.

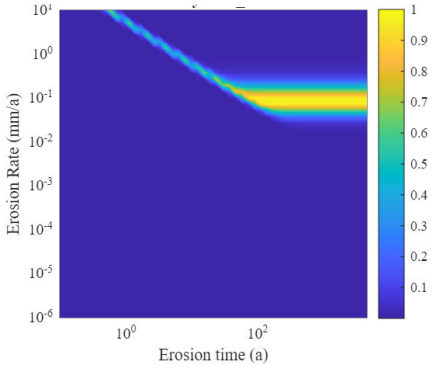

Figure 4: (a) The probability likelihood surface plot of $\dot{\varepsilon}$-t_s 2500 pairs in log-space. The light greenish-blue shaded sloped portion points towards a mildly fitting possible transient-state solution. The yellow-shaded patch represents the possible steady-state solutions.

4 Performance of CoRSEER

We tested all three modules of CoRSEER for the natural data available in the literature (Smedley et al., 2021; Brill et al., 2021; Balco et al., 2023; Lehmann et al., 2019a; Lehmann et al., 2019b; Luo et al., 2018) to: i) benchmark the app's in-built parameters for performance, accuracy, and flexibility, and ii) to understand how CoRSEER's mathematical framework and algorithmic implementation influence the final result. We derive: i) Calibration parameters ($\overline{\sigma\varphi_0}$ and μ) for the calibration samples of Smedley et al. (2021), Brill et al. (2021), Balco et al. (2023), Lehmann et al. (2019a), Lehmann et al. (2019b), Luo et al. (2018) using CoRSEER-I. ii) Apparent ages (t_{app}) for Smedley et al. (2021), Brill et al. (2021), Lehmann et al. (2019b), Luo et al. (2018) (there was no usable unknown age LDP for the remaining dataset) using CoRSEER-II. iii) The erosion rates for Smedley et al. (2021), Lehmann et al. (2019b), using CoRSEER-III, as both studies have a well-established dataset of erosion history. The complete methodology for deriving the required parameters is provided in Section 3. We must mention that all operations were performed using the FOK model (r = 1), as all the literature data were analysed previously using FOK. However, CoRSEER has the flexibility of using r>1.

https://doi.org/10.5194/egusphere-2026-1303
Preprint. Discussion started: 26 March 2026

4.1 Calibration:

Across the published calibration dataset, CoRSEER-I generally reproduces literature calibration parameters, with the best agreement observed for Lehman et al. (2019a) and Luo et al. (2022), where the CoRSEER-I-derived $\log_{10}(\overline{\sigma\varphi_0})$ and μ values are broadly comparable to reported estimates. This agreement is consistent with a similar normalisation choice for the L_x/T_x depth profiles. In contrast, several datasets show systematic offsets between CoRSEER-I and the literature values. For example, in Balco et al. (2023), the sample IR50_KAY_110, the calibration parameters shifts to higher values, from $\log_{10}(\overline{\sigma\varphi_0})$ = -7.30 and μ = 0.34 mm^{-1} to -6.58 and 0.51 mm^{-1} whereas for the sample pIRIR225_KAY_110 shifts to lower values, from -7.68 and 0.54 mm^{-1} to 7.77 and 0.36 mm^{-1}. In Brill et al. (2021), CoRSEER-I predicted decreased calibration parameters for IR50_HAR1-1_CAL but increased parameters for IR50_TEM3-1_CAL and IR50_VAL4-1_CAL1. For the two calibration samples for which Brill et al. (2021) did not report the final parameters (IR50_RAB5-1_CAL and IR50_VAL4-1_CAL2), CoRSEER-I yielded -7.38, 0.76 mm^{-1} and -7.50, 0.37 mm^{-1}, respectively. In Smedley et al. (2021), the ROAD set was dominated by a decrease in both parameters with two clear increased cases (IR50_ROAD1 and IR50_ROAD3). Lehmann et al. (2018) show predominantly decreased parameters for MBMB samples, with one increased case (IR50_MBMV7) and one near-balanced case (IR50_MBMV1). We attribute these discrepancies primarily to 1) differences in the fitting strategy, 2) differences in the L_x/T_x normalisation (manual plateau selection versus automated normalisation) and 3) both the $\overline{\sigma\varphi_0}$ and μ may slightly covary during optimisation of best fitting . The range of $log_{10}(\overline{\sigma\varphi_0})$ and μ values predicted by CoRSEER-I are -8.41 to -4.82 and 0.36 to 3.36 mm^{-1} (Table 3), showing the plausible flexibility of the app for a wide variety of exposure conditions and lithology.

We plotted CoRSEER-I vs. the literature dataset and evaluated the R^2 value with respect to the 1:1 line to summarise the compilation-scale performance for 23 samples. In Fig. 5a, μ_{CoRSEER} versus $\mu_{\text{literature}}$ gives $R^2_{1:1} = 0.562$ for $n = 23$, meaning CoRSEER-I tracks published μ values moderately well, even though a large fraction of points falls below the 1:1 line. In Fig. 5b, $\overline{\sigma\varphi_0}_{\text{CoRSEER}}$ versus $\overline{\sigma\varphi_0}_{\text{literature}}$ gives $R^2_{1:1} = 0.316$ for $n = 23$, showing weaker agreement and stronger scatter. It is well established that the $\overline{\sigma\varphi_0}$ and μ covary and we present the relationship between them in Supplementary Section S8. To investigate the offset between the established calibration parameters and underlying reason behind it we plot $(\log_{10}(\overline{\sigma\varphi_0})/\mu)_{\text{CoRSEER}}$ vs $(\log_{10}(\overline{\sigma\varphi_0})/\mu)_{\text{literature}}$ in Fig. 5c which gives $R^2_{1:1} = 0.379$ showing weaker agreement. This explains that the offset of calibration parameters is contributed weakly by covariance and dominantly by normalisation and fitting strategy for calibration. Visually, most points fall below the 1:1 line in both panels, so the dominant overall tendency in this compilation is that CoRSEER estimates lower μ and $\overline{\sigma\varphi_0}$ than literature for many samples, while a smaller set of samples shows the opposite paired behaviour.

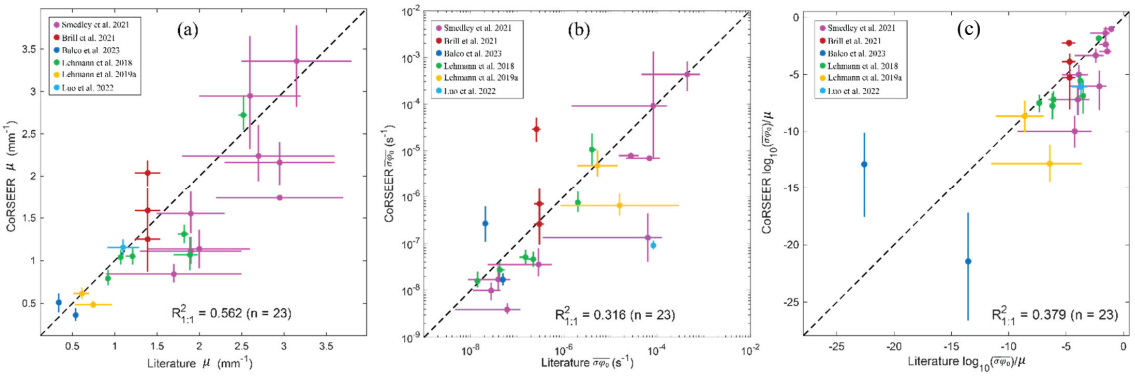

Figure 5: The 1:1 comparison between CoRSEER-I and literature calibration parameters. The round filled circles show the median/best fitting values, and the solid lines represent the respective ± δ values, which are plotted along with the black dotted 1:1 correlation line. (a) Attenuation coefficients (μ) (b) bleaching rates ($\overline{\sigma\varphi_0}$) and (c) The ratio $\log_{10}(\overline{\sigma\varphi_0})/\mu$ for all compiled calibration samples ($n = 23$).

Table 3: List of literature and corresponding sample modelling parameters derived from both literature and CoRSEER.

Author	Samples	$\dot{D}$ (Gy /kyr)	D_o (Gy)	Location	Rock Type	Sampling Type	Known age (as)	$log_{10}(\overline{\sigma\varphi}_{o,CoRSEER})$			$log_{10}(\overline{\sigma\varphi}_{o,literature})$			$\mu_{CoRSEER}$ (mm^{-1})			$\mu_{literature}(mm^{-1})$		
								-1δ	BF/M	$+1\delta$	-1δ	BF/M	$+1\delta$	-1δ	BF/M	$+1\delta$	-1δ	BF/M	$+1\delta$
Balco et al. (2023)	IR50_KAY_110	-	-	Kay Peak Ridge, West Antarctica	Biotite gneiss	Surface bedrock of The ice sheet free portion	4	-6.97	-6.58	-6.21	*	-7.30	*	0.40	0.51	0.61	*	0.34	*
	pIRIR225_KAY_110	-						-7.89	-7.77	-7.63	*	-7.68	*	0.30	0.36	0.44	*	0.54	*
Brill et al. (2021)	IR50_HAR 1-1 CAL	0.53	500	Harhoura, Morocco	Calcarenite, Carbonate Limestone	Coastal Boulders	2.15	-7.02	-6.59	-6.20	-6.64	-6.52	-6.43	0.87	1.25	1.60	1.24	1.39	1.54
	IR50_RAB 5-1 CAL	-		Rabat, Morocco				-7.60	-7.38	-7.16	*	*	*	0.52	0.76	0.97	*	*	*
	IR50_TEM 3-1 CAL	0.51		Temara, Morocco				-4.82	-4.54	-4.30	-5.68	-5.58	-5.50	1.88	2.04	2.18	1.24	1.39	1.54
	IR50_VAL 4-1 CAL 1	-		Val d'Or, Morocco				-6.50	-6.16	-5.84	-6.64	-6.52	-6.43	1.29	1.59	1.85	1.24	1.39	1.54
	IR50_VAL 4-1 CAL 2	-		Val d'Or Morocco				-7.57	-7.50	-7.44	*	*	*	0.33	0.37	0.41	*	*	*
Lehmann et al. (2018)	IR50_MBMV1	-	-	Mer de Glace, Mont Blanc Massif, France	Gneiss	Bedrock outcrop	137	-7.94	-7.80	-7.60	-7.89	-7.85	-7.82	0.95	1.04	1.13	1.05	1.07	1.08
	IR50_MBMV6				Gneiss		2	-6.33	-6.13	-5.89	-5.74	-5.70	-5.66	0.71	0.79	0.89	0.92	0.92	0.95
	IR50_MBMV7				Granite		69	-5.32	-4.98	-4.64	-5.44	-5.40	-5.30	2.55	2.72	2.95	2.46	2.52	2.56
	IR50_MBMV8				Gneiss		3	-7.50	-7.34	-7.18	-6.82	-6.66	-6.62	0.89	1.07	1.28	1.70	1.89	1.98
	IR50_MBMV10				Gneiss		18	-7.43	-7.30	-7.14	-6.96	-6.82	-6.82	1.20	1.31	1.42	1.75	1.82	1.87
	IR50_MBMV11				Gneiss		30	-7.72	-7.57	-7.40	-7.41	-7.38	-7.28	0.96	1.05	1.15	1.13	1.21	1.22
Lehmann et al. (2019a)	IR50_MBTP7_CAL	-	-		Granite	Bedrock	2	-5.57	-5.33	-5.00	-5.71	-5.65	-4.84	0.55	0.61	0.68	0.51	0.53	0.69
	IR50_MBTP8_CAL				Granite		11	-6.40	-6.19	-5.94	-6.07	-5.92	-3.53	0.44	0.48	0.53	0.53	0.53	0.97
Luo et al. (2022)	pIRIR175_LS_1K_CAL	3.3	506	Langshan Normal Fault, Inner Mongolia, China	Granite	Fault Scarp	3	-7.13	-7.05	-6.94	-7.081	-7.078	-7.076	1.06	1.16	1.25	0.91	1.10	1.29
Smedley et al. (2021)	IR50_ROAD01	4.81	-	NW Scotland, roadcut	Torridonian sandstone	Insitu Bedrock	0.01	-3.72	-3.37	-3.09	-4.33	-3.55	-3.08	2.82	3.36	3.78	2.50	3.20	3.80
	IR50_ROAD02	4.76	-				57	-7.40	-6.88	-6.36	-6.46	-5.18	-3.90	0.91	1.14	1.36	1.40	2.10	2.60
	IR50_ROAD03	4.00	-				44	-5.15	-4.04	-2.88	-5.83	-4.81	-3.79	2.32	2.95	3.66	2.00	2.70	3.20
	IR150_ROAD01	4.81	-				0.01	-5.20	-5.17	-5.13	-4.67	-4.49	-3.94	1.60	1.74	1.89	2.20	3.10	3.70
	IR150_ROAD02	4.76	-				57	-8.02	-7.77	-7.49	-8.06	-7.76	-7.16	1.32	1.55	1.81	1.50	1.90	2.30
	IR150_ROAD03	4.00	-				44	-8.21	-8.01	-7.84	-7.95	-7.42	-7.36	0.96	1.11	1.28	1.30	1.90	2.50
	IR225_ROAD01	4.81	-				0.01	-5.16	-5.11	-5.06	-4.82	-4.54	-4.40	1.97	2.16	2.40	2.30	3.00	3.60
	IR225_ROAD02	4.76	-				57	-7.70	-7.45	-7.11	-7.64	-7.05	-6.26	1.94	2.24	2.61	1.80	2.80	3.60
	IR225_ROAD03	4.00	-				44	-8.51	-8.41	-8.27	-8.33	-7.77	-6.93	0.75	0.84	0.96	0.90	1.40	2.50

https://doi.org/10.5194/egusphere-2026-1303
Preprint. Discussion started: 26 March 2026

4.2 Exposure Age:

We evaluated the apparent exposure ages (t_{app}) of the unknown age LDPs of the literature dataset using CoRSEER-II for 41 samples. As the evaluated age exclusively depends on the chosen calibration samples, dose rate, and characteristic dose, we follow the same pattern as given in the literature dataset, except for a few, as mentioned further. Lehmann et al. (2019b) used a combined calibration parameter of IR50_MBTP7_CAL (2 as) and IR50_MBTP8_CAL (11 as), whereas the CoRSEER-I can only do a single calibration. Thus, we used IR50_MBTP7_CAL, as it closely resembles the calibration parameters in the literature. Brill et al. (2021) used CoRSEER-I to evaluate the parameters of IR50_RAB 5-1 CAL for the samples of IR50_RAB 1-1, IR50_RAB 1-2, and IR50_RAB 5-1 (these samples were evaluated using IR50_HAR 1-1 CAL I in the literature due to the large uncertainty in IR50_RAB 5-1 CAL). We plotted the CoRSEER-II vs literature apparent age dataset and evaluated the R^2 value with respect to the 1:1 line to summarise the compilation-scale performance. Interestingly, the evaluated t_{app} using CoRSEER-II is comparable to the literature and falls closely around the 1:1 line (Fig. 6) despite a significant difference in the calibration parameters used in this study. The derived $R^2_{1:1} = 0.889$ represents the CoRSEER-II track, which has apparent exposure ages with high certainty. There was a significant underestimation by CoRSEER-II for the IR50_RAB 1-1, IR50_RAB 5-1 and IR50_TEM 2-1. This is due to the following reasons: 1) a change in the calibration sample, as mentioned earlier. 2) The high SCF normalisation factors a = 1.1 (up to 10%) of the sigmoidal fitting for the IR50_TEM 2-1, which might have changed the position of $x_{0.5}$.

The range of t_{app} values predicted by CoRSEER-II is 1 a to 8.5 ka (Table 4), showing its potential as a decadal-to-millennial chronometric mathematical tool for RSLD.

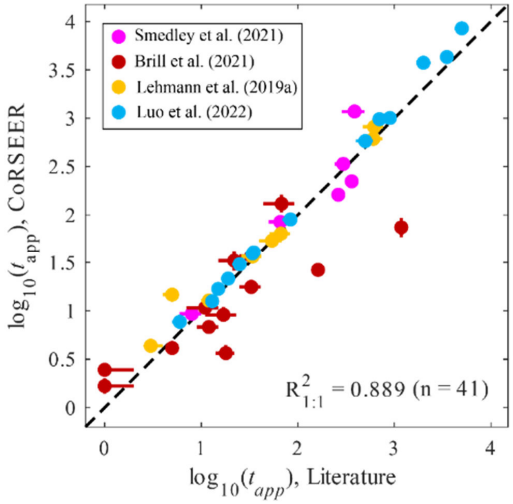

Figure 6: The 1:1 comparison between CoRSEER-II and literature t_{app} data. The round filled circles show the median/best fitting values, and the solid lines represent the respective ± δ values, which are plotted along with the black dotted 1:1 correlation line.

Table 4: Representation of exposure ages for samples evaluated from both the literature and CoRSEER.

Author	Unknown age Samples	t_{app} *literature*			t_{app} CoRSEER		
		-1δ	*BF/M*	*+1δ*	*-1δ*	*BF/M*	*+1δ*
Brill et al. (2021)	IR50_HAR 1-1	5	5	5	4	4	4
	IR50_HAR 2-1	11	17	23	8	9	11
	IR50_HAR 3-1	25	33	41	15	18	21
	IR50_RAB 1-1	141	162	183	23	26	30
	IR50_RAB 1-2	9	12	15	8	9	10
	IR50_RAB 5-1	1022	1180	1338	59	74	93
	IR50_TEM 2-1	14	18	22	3	4	4
	IR50_TEM 3-1	1	1	2	2	2	3
	IR50_TEM 4-1	1	1	2	1	2	2
	IR50_VAL 1-1	15	22	29	26	33	42

https://doi.org/10.5194/egusphere-2026-1303
Preprint. Discussion started: 26 March 2026

	IR50_VAL 1-2	7	11	15	9	11	13
	IR50_VAL 4-1	44	68	92	106	130	162
	IR50_VAL 6-1	25	33	41	32	37	42
Lehmann et al., (2019)	IR50_MBAM1	26	34	42	31	36	43
	IR50_MBAM2	51	67	83	61	64	67
	IR50_MBAM3	10	12	14	12	13	13
	IR50_MBTP1	471	618	765	690	813	962
	IR50_MBTP2	462	606	750	537	612	697
	IR50_MBTP5	4	5	5	14	15	16
	IR50_MBTP9	40	54	68	49	54	60
	IR50_MBTP11	3	3	4	4	4	5
Luo et al.(2022)	pIRIR175_LS0_10	13	13	13	12	13	14
	pIRIR175_LS30_40	14	15	16	16	17	18
	pIRIR175_LS70_80	31	34	37	37	39	41
	pIRIR175_LS90-100	32	35	38	39	41	43
	pIRIR175_LS140_150	5	6	7	7	8	9
	pIRIR175_LS160_170	69	84	99	81	90	98
	pIRIR175_LS210_220	21	25	29	26	30	34
	pIRIR175_LS290_300	17	19	21	21	21	22
	pIRIR175_LS310_320	600	700	800	881	978	1082
	pIRIR175_LS370_380	800	900	1000	951	1003	1057
	pIRIR175_LS390_400	400	500	600	533	581	635
	pIRIR175_LS420_430	4200	5000	5800	7591	8503	9508
	pIRIR175_LS450_460	3000	3500	4000	3800	4299	4866
	pIRIR175_LS590_600	1700	2000	2300	3520	3745	3985
Smedley et al. (2021)	IR50_BALL02	6	8	10	8	9	11
	IR50_BALL03	284	387	490	1165	1174	1183
	IR150_BALL02	50	66	82	77	85	92
	IR150_BALL03	242	296	350	303	337	374
	IR225_BALL02	233	263	293	149	162	176
	IR225_BALL03	313	362	411	201	223	246

4.3 Erosion Rates

Here we establish the steady-state erosion rate ($\dot{\varepsilon}_{ss}$) and corresponding onset time of erosion (t_{ss}) of literature dataset (n = 11) using CoRSEER-III. We carefully chose the calibration and dose parameters, as mentioned in the earlier sections. The choice of sample for analysis assumes that these samples are in a steady state, as described in the literature(Lehmann et al., 2019a; Smedley et al., 2021). $\dot{\varepsilon}_{ss}$ and t_{ss} are well documented. We found extremely good agreement between CoRSEER-III and the literature-derived erosion history, as documented in Table 5. When the sample is in a transient state, one can visually identify the solution that generally lies in the sloped portion of the $\dot{\varepsilon}_{ss}$ vs t_{ss} likelihood plot. It is mathematically challenging to produce an objective method to control a pair of possible solutions. Thus, we do not present any transient-state condition scenarios. But it is possible to derive a transient state solution from CoRSEER-III if onset of erosion (t_s) is known by some means.

Table 5: Representation of steady-state exposure age and erosion rates for samples evaluated from both the literature and CoRSEER.

Author	Samples	$\dot{\varepsilon}_{ss,literature}$ (mm/a)	$\dot{\varepsilon}_{ss,CoRSEER-III}$ (mm/a)	$t_{ss,literature}(a)$	$t_{ss,CoRSEER-III}$ (a)
Lehmann et al. (2019b)	IR50_MBAM1	0.057	0.072	285	171
	IR50_MBAM2	0.028	0.037	461	240
	IR50_MBAM3	0.2	0.27	56	52
	IR50_MBTP1	0.0035	0.0027	2610	2430
	IR50_MBTP2	0.0035	0.0052	3146	1357
	IR50_MBTP5	0.3	0.37	64	24.42
	IR50_MBTP6	4.3	4.63	4	4
	IR50_MBTP9	0.032	0.037	486	471
	IR50_MBTP11	0.53	0.52	42	31
Smedley et al., (2021)	IR50_BALL02	0.066	0.1	73	88
	IR150_BALL02	0.009	0.01	593	390

https://doi.org/10.5194/egusphere-2026-1303
Preprint. Discussion started: 26 March 2026

5 Discussion

The RSLD is a promising potential chronometer of geological processes which occur under sufficient sunlight. Rigorous methodological development and precise field application of RSLD can cause a paradigm shift in surface exposure chronometry by enabling us to date decadal to millennial exposure events. Furthermore, it can accurately establish steady-state in situ erosion rates. Thus, the CoRSEER attempts to improve the application, standardisation, and intercomparison of results among several studies.

5.1 Preliminary precautions:

Large scatter in the luminescence depth profile (LDP) and high fractional uncertainty in L_x/T_x make plateau identification unreliable and reduce the stability of any inversion (i.e., the SCF normalisation, estimation of calibration parameters, exposure age, erosion rates). We can reduce L_x/T_x uncertainty by adopting a modified post-infrared infrared stimulated luminescence protocol with lower heating rates and longer isothermal holding times (Jenkins et al., 2018), and by using metal cups (Elkadi et al., 2021). It is recommended for the same sample to measure two or more LDPs and maintain millimetre-scale sampling density with substantial fraction of points located on the sigmoidal transition. Importantly, the fractional error structure should be similar or random with depth; if the fractional error at lower depths is systematically higher than at higher depths, the fitting becomes biased toward the plateau, and the inferred parameters become unreliable. Although we cannot yet provide a statistical criterion for the required fraction of points on the sigmoidal part of the curve, based on our observation of Fig. 2a and Fig. 3a we recommend that more than 50% of all L_x/T_x measurement points should lie before the final plateau. If the measured profile is dominated by plateau points, we recommend reducing the measurement depth such that the total number of points on the initial plateau and sigmoidal region exceeds 50% of the total.

In the case of incomplete LDP, the maximum measurement depth is lower than steady-state depth, it impossible to reconstruct the plateau point. Although it is recommended to measure L_x/T_x upto the equilibrium depth (which is the stable plateau). Similarly, for the large scatter in experimental data, it is difficult to identify the plateau manually. The SCF and parameter estimation to normalise the LDP is a major step forward as it resolves these both issues and removes the manual intervention from mathematical inversion, thereby improving the accuracy of fitting (Fig. 1e).

5.2 Calibration

While using CoRSEER-I, we suggest that there are a few precautions we must take to estimate $\overline{\sigma\varphi}_{\circ}$ and μ accurately. If the IRSL signal from feldspar minerals is used for LDP measurements, we suggest evaluating the order of kinetics (r) beforehand and incorporating it into the calculation. The application of FOK can cause severe underestimation and overestimation of the exposure age and erosion rate (Biswas et al., 2023; Pathan et al., 2024). The different methods for evaluating the r value are thoroughly discussed in Biswas et al. (2023) and Pathan et al. (2024). Furthermore, if the calibration sample is young (say 1-10(a), for example, a known-age deglaciated surface or manually exposed surface created by chipping off a boulder face, the LDP is assumed to have no effect of erosion. In contrast, when using older natural calibration samples (t >100 years), erosion is expected to affect LDP significantly (Lehmann et al., 2018; Smedley et al., 2021), and it further dominates in high-eroding environments. This can significantly underestimate the $\overline{\sigma\varphi}_{\circ}$ and mildly affect the μ. This is inferred from the samples IR50_MBMV1 (t = 137a) and IR50_MBMV6 (t = 2), which were samples from the same site with similar lithology, but the $\log \overline{\sigma\varphi}_{\circ}$ was estimated as -7.8 and -6.13, respectively which is two orders of magnitude difference, whereas μ was estimated at 1.04 and 0.8 mm^{-1}. Thus, the erosion rate must be explicitly incorporated into CoRSEER-I. To avoid this complexity and reduce model dependence on uncertain erosion histories, it is recommended to use young calibration surfaces at sampling sites where there is no erosion over the period of interest. This allows for the precise calibration of kinetic parameters under well-constrained exposure conditions. This will further remove any ambiguity due to changes in decay kinetics, lithology, surface orientation, shielding, and light penetration.

https://doi.org/10.5194/egusphere-2026-1303
Preprint. Discussion started: 26 March 2026

Although our present modelling framework focuses on single calibration (SC), it is worth noting that multi-calibration strategies (MC) can be highly effective under certain conditions. When multiple calibration samples of different known ages, but from the same lithology and sunlight exposure conditions, are available, it becomes possible to constrain $\overline{\sigma\varphi}_{\circ}$, μ and r simultaneously (Pathan et al., 2024). However, the accuracy of such multi-calibration is strongly dependent on the number of calibration samples and their age spread. A wider temporal distribution across well-characterised surfaces enhances the resolution of the kinetic behaviour. While we recognise the potential of this methodology, it lies beyond the scope of the current work and is not implemented in the present version of CoRSEER.

5.3 Apparent Age Estimation:

After estimation of kinetic parameters, the estimation of exposure and erosion history appears to be highly dependent on the position of the $x_{0.5}$. There are two possible scenarios:

Case 1 : For non-eroding exposure conditions if the depth of half saturation of the LDP, $x_{0.5}$ is smaller than $x_{0.5,max}$ then the apparent exposure age is equal to actual exposure age of the sample and if $x_{0.5,max} < x_{0.5} \leq x_{0.5,ss}$ then the sample is reached to steady-state and the exposure age is greater than the t_{max}, maximum dateable exposure age.

Case 2: If the derived apparent ages are highly underestimated than the expected age (derived using an independent method) then there is presence of erosion which was seen in the sample IR50_BALL02 (Smedley et al., 2021). CoRSEER-III should be used to further re-establish the exposure-erosion history. Furthermore, when using IRSL to establish the LDP, the r value should be the same for calibration and unknown samples (Pathan et al., 2024). We incorporated all these modelling aspects, diagnostics, and interpretation into the input and output GUI plots (Fig. 3).

5.4 Erosion Rate estimation:

The fundamental assumptions and modelling aspects which build CoRSEER-III were taken from Lehmann et al. (2019a), where the authors coupled ^{10}Be concentration and the LDP to evaluate the erosion-corrected ^{10}Be exposure age range. The main difference is that CoRSEER-III does not incorporate ^{10}Be concentration; rather, it incorporates independent exposure age i) which can be derived from an independent dating method or ii) by incorporating t_{max} from forward modelling of $x_{0.5}$ vs t.

6 Conclusion

In this study, we present CoRSEER as an integrated, reproducible workflow for RSLD that converts the LDP into physically interpretable exposure and erosion information. CoRSEER reduces user-dependent choices by automating key steps that vary across studies. CoRSEER presents three linked modules: (i) calibration of site- and lithology-specific bleaching parameters, (ii) apparent exposure age estimation, and (iii) erosion rate estimation under steady-state scenarios. Reanalysis of published datasets shows that CoRSEER-I generally reproduces plausible calibration parameter estimates and captures literature trends, while also presenting systematic offsets in some datasets that mainly arise from differences in normalisation and fitting strategy. Despite these calibration differences, CoRSEER-II yields apparent exposure ages that closely track published values with strong 1:1 agreement, demonstrating that the platform provides robust chronometric outputs when input calibration parameters are followed as reference studies. Finally, CoRSEER-III reproduces steady-state erosion histories with excellent agreement for well-constrained erosion datasets, supporting its use as a quantitative erosion-rate estimator when exposure age constraints are available, and the profile indicates steady-state behaviour. These results support the central conclusion that objective normalisation and standardised inversion materially improve reproducibility in RSLD without reducing model flexibility. CoRSEER enables consistent decadal-to-millennial exposure reconstructions and strengthens its practical use, but there are a few limitations which must be addressed. The CoRSEER performance depends on data quality, that is, a significant number of L_x/T_x sampling across the sigmoidal slope and lesser L_x/T_x error estimates remain essential, and shallow or plateau-dominated profiles can bias sigmoidal fitting. The current release prioritises

https://doi.org/10.5194/egusphere-2026-1303
Preprint. Discussion started: 26 March 2026

single-sample calibration and does not yet implement multi-calibration optimisation, and the objective selection of transient-state erosion solutions remains mathematically challenging and therefore user-guided. Future versions should (i) implement multi-calibration strategies to constrain kinetic parameters jointly and (ii) expand diagnostics that flag profiles likely to be poorly constrained.

7 Code availability

CoRSEEr (Calculator of Rock Surface Exposure Age and Erosion Rates) was released as open-source software and archived on Zenodo. The exact version used in this study is CoRSEEr v 0.1.0 (Zenodo version DOI: https://doi.org/10.5281/zenodo.18434547). The source repository is hosted on GitHub at https://github.com/arbazNP/CoRSEERv1 .

8 Competing Interest

The authors declare no conflicts of interest.

9 Author Contribution

AP contributed to conceptualization, data curation, formal analysis, investigation, methodology, project administration, software, validation, visualization, writing of the original draft, and review and editing of the manuscript. RHB contributed to conceptualization, methodology, project administration, resources, supervision, writing of the original draft, and review and editing of the manuscript. DK contributed to resources and review and editing of the manuscript.

10 References

Balco, G., Stone, J. O., Lifton, N. A., and Dunai, T. J.: A complete and easily accessible means of calculating surface exposure ages or erosion rates from 10Be and 26Al measurements, Quaternary Geochronology, 3, 174–195, https://doi.org/10.1016/j.quageo.2007.12.001, 2008.

Balco, G., Brown, N., Nichols, K., Venturelli, R. A., Adams, J., Braddock, S., Campbell, S., Goehring, B., Johnson, J. S., Rood, D. H., Wilcken, K., Hall, B., and Woodward, J.: Reversible ice sheet thinning in the Amundsen Sea Embayment during the Late Holocene, The Cryosphere, 17, 1787–1801, 10.5194/tc-17-1787-2023, 2023.

Biswas, R. H., Pathan, A. N., and Malik, J. N.: General order kinetics model for OSL rock surface exposure dating, Proceedings of the Indian National Science Academy, 89, 644–654, 10.1007/s43538-023-00172-y, 2023.

Brill, D., May, S. M., Mhammdi, N., King, G., Lehmann, B., Burow, C., Wolf, D., Zander, A., and Brückner, H.: Evaluating optically stimulated luminescence rock surface exposure dating as a novel approach for reconstructing coastal boulder movement on decadal to centennial timescales, Earth Surface Dynamics, 9, 205–234, 10.5194/esurf-9-205-2021, 2021.

Brown, N. D. and Moon, S.: Revisiting erosion rate estimates from luminescence profiles in exposed bedrock surfaces using stochastic erosion simulations, Earth and Planetary Science Letters, 528, 115842, 10.1016/j.epsl.2019.115842, 2019.

Burbank, D. W., Leland, J., Fielding, E., Anderson, R. S., Brozovic, N., Reid, M. R., and Duncan, C.: Bedrock incision, rock uplift and threshold hillslopes in the northwestern Himalayas, Nature, 379, 505–510, 1996.

Chen, R. and Leung, P. L.: The decay of OSL signals as stretched-exponential functions, Radiation Measurements, 37, 519–526, https://doi.org/10.1016/S1350-4487(03)00007-6, 2003.

Colman, S. M.: Rock-weathering rates as functions of time, Quaternary Research, 15, 250–264, https://doi.org/10.1016/0033-5894(81)90029-6, 1981.

Desilets, D. and Zreda, M.: Spatial and temporal distribution of secondary cosmic-ray nucleon intensities and applications to in situ cosmogenic dating, Earth and Planetary Science Letters, 206, 21–42, https://doi.org/10.1016/S0012-821X(02)01088-9, 2003.

Duller, G. A. T.: Behavioural studies of stimulated luminescence from feldspars, Radiation Measurements, 27, 663–694, https://doi.org/10.1016/S1350-4487(97)00216-3, 1997.

Dunai, T. J.: Scaling factors for production rates of in situ produced cosmogenic nuclides: a critical reevaluation, Earth and Planetary Science Letters, 176, 157–169, https://doi.org/10.1016/S0012-821X(99)00310-6, 2000.

Dunai, T. J.: Cosmogenic nuclides: principles, concepts and applications in the earth surface sciences, Cambridge University Press2010.

Durcan, J. A., King, G. E., and Duller, G. A.: DRAC: Dose Rate and Age Calculator for trapped charge dating, Quaternary Geochronology, 28, 54–61, 2015.

https://doi.org/10.5194/egusphere-2026-1303
Preprint. Discussion started: 26 March 2026

Elkadi, J., Lehmann, B., King, G. E., Steinemann, O., Ivy-Ochs, S., Christl, M., and Herman, F.: Quantification of post-glacier bedrock surface erosion in the European Alps using 10Be and optically stimulated luminescence exposure dating, Earth Surface Dynamics, 10, 909–928, 10.5194/esurf-10-909-2022, 2022.

Freiesleben, T. H., Thomsen, K. J., and Jain, M.: Novel luminescence kinetic models for rock surface exposure dating, Radiation Measurements, 160, 106877, 10.1016/j.radmeas.2022.106877, 2023.

Ganti, V., Von Hagke, C., Scherler, D., Lamb, M. P., Fischer, W. W., and Avouac, J.-P.: Time scale bias in erosion rates of glaciated landscapes, Science Advances, 2, e1600204, 2016.

Gliganic, L. A., Meyer, M. C., Sohbati, R., Jain, M., and Barrett, S.: OSL surface exposure dating of a lithic quarry in Tibet: Laboratory validation and application, Quaternary Geochronology, 49, 199–204, 10.1016/j.quageo.2018.04.012, 2019.

Guralnik, B., Li, B., Jain, M., Chen, R., Paris, R. B., Murray, A. S., Li, S.-H., Pagonis, V., Valla, P. G., and Herman, F.: Radiation-induced growth and isothermal decay of infrared-stimulated luminescence from feldspar, Radiation Measurements, 81, 224–231, 10.1016/j.radmeas.2015.02.011, 2015.

Jain, M., Sohbati, R., Guralnik, B., Murray, A. S., Kook, M., Lapp, T., Prasad, A. K., Thomsen, K. J., and Buylaert, J. P.: Kinetics of infrared stimulated luminescence from feldspars, Radiation Measurements, 81, 242–250, https://doi.org/10.1016/j.radmeas.2015.02.006, 2015.

Kaufmann, K. W.: Fitting and using growth curves, Oecologia, 49, 293–299, 1981.

Lal, D.: Cosmic ray labeling of erosion surfaces: in situ nuclide production rates and erosion models, Earth and Planetary Science Letters, 104, 424–439, https://doi.org/10.1016/0012-821X(91)90220-C, 1991.

Laskaris, N. and Liritzis, I.: A new mathematical approximation of sunlight attenuation in rocks for surface luminescence dating, Journal of Luminescence, 131, 1874–1884, https://doi.org/10.1016/j.jlumin.2011.04.052, 2011.

Lehmann, B., Valla, P. G., King, G. E., and Herman, F.: Investigation of OSL surface exposure dating to reconstruct post-LIA glacier fluctuations in the French Alps (Mer de Glace, Mont Blanc massif), Quaternary Geochronology, 44, 63–74, 10.1016/j.quageo.2017.12.002, 2018.

Lehmann, B., Herman, F., Valla, P. G., King, G. E., and Biswas, R. H.: Evaluating post-glacial bedrock erosion and surface exposure duration by coupling in situ optically stimulated luminescence and 10Be dating, Earth Surface Dynamics, 7, 633–662, 10.5194/esurf-7-633-2019, 2019a.

Lehmann, B., Herman, F., Valla, P. G., King, G. E., Biswas, R. H., Ivy-Ochs, S., Steinemann, O., and Christl, M.: Postglacial erosion of bedrock surfaces and deglaciation timing: New insights from the Mont Blanc massif (western Alps), Geology, 48, 139–144, 10.1130/g46585.1, 2019b.

Lifton, N., Sato, T., and Dunai, T. J.: Scaling in situ cosmogenic nuclide production rates using analytical approximations to atmospheric cosmic-ray fluxes, Earth and Planetary Science Letters, 386, 149–160, https://doi.org/10.1016/j.epsl.2013.10.052, 2014.

Luo, M., Chen, J., Gong, Z., Owen, L. A., Yang, H., Jiang, X., Yin, J., Xu, W., and Wang, H.: A new surface rupture of the 1556 Huaxian M~ 8.5 earthquake revealed by rock surface luminescence dating of a bedrock fault scarp and colluvial wedges, Geophysical Research Letters, 53, e2025GL119878, 2026.

Luo, M., Chen, J., Liu, J., Qin, J., Owen, L. A., Han, F., Yang, H., Wang, H., Zhang, B., Yin, J., and Li, Y.: A test of rock surface luminescence dating using glaciofluvial boulders from the Chinese Pamir, Radiation Measurements, 120, 290–297, 10.1016/j.radmeas.2018.07.017, 2018.

Molnar, P. and England, P.: Late Cenozoic uplift of mountain ranges and global climate change: chicken or egg?, Nature, 346, 29–34, 10.1038/346029a0, 1990.

Owen, L. A. and Dortch, J. M.: Nature and timing of Quaternary glaciation in the Himalayan–Tibetan orogen, Quaternary Science Reviews, 88, 14–54, 2014.

Pathan, A. N., Biswas, R. H., Lehmann, B., King, G. E., and Herman, F.: Towards accurate modelling of rock surface exposure dating using luminescence to estimate post-exposure erosion rate, Quaternary Geochronology, 85, 101634, https://doi.org/10.1016/j.quageo.2024.101634, 2024.

Schaefer, J. M., Codilean, A. T., Willenbring, J. K., Lu, Z.-T., Keisling, B., Fülöp, R.-H., and Val, P.: Cosmogenic nuclide techniques, Nature Reviews Methods Primers, 2, 18, 10.1038/s43586-022-00096-9, 2022.

Smedley, R. K., Small, D., Jones, R. S., Brough, S., Bradley, J., and Jenkins, G. T. H.: Erosion rates in a wet, temperate climate derived from rock luminescence techniques, Geochronology, 3, 525–543, 10.5194/gchron-3-525-2021, 2021.

Sohbati, R. and Hippe, K.: OSL-14C-10Be: A novel composite geochronometer for simultaneous quantification of timing and magnitude of change in bedrock outcrop erosion rate, Earth Surface Processes and Landforms, 48, 322–331, https://doi.org/10.1002/esp.5487, 2023.

Sohbati, R., Jain, M., and Murray, A.: Surface exposure dating of non-terrestrial bodies using optically stimulated luminescence: A new method, Icarus, 221, 160–166, 10.1016/j.icarus.2012.07.017, 2012a.

Sohbati, R., Murray, A. S., Chapot, M. S., Jain, M., and Pederson, J.: Optically stimulated luminescence (OSL) as a chronometer for surface exposure dating, Journal of Geophysical Research: Solid Earth, 117, 10.1029/2012jb009383, 2012b.

Sohbati, R., Murray, A. S., Jain, M., Buylaert, J.-P., and Thomsen, K. J.: Investigating the resetting of OSL signals in rock surfaces, Geochronometria, 38, 249–258, 10.2478/s13386-011-0029-2, 2011.

Sohbati, R., Liu, J., Jain, M., Murray, A., Egholm, D., Paris, R., and Guralnik, B.: Centennial- to millennial-scale hard rock erosion rates deduced from luminescence-depth profiles, Earth and Planetary Science Letters, 493, 218–230, 10.1016/j.epsl.2018.04.017, 2018.

Stone, J. O.: Air pressure and cosmogenic isotope production, Journal of Geophysical Research: Solid Earth, 105, 23753–23759, https://doi.org/10.1029/2000JB900181, 2000.

https://doi.org/10.5194/egusphere-2026-1303
Preprint. Discussion started: 26 March 2026

550 Wintle, A. G. and Murray, A. S.: A review of quartz optically stimulated luminescence characteristics and their relevance in single-aliquot regeneration dating protocols, Radiation Measurements, 41, 369–391, https://doi.org/10.1016/j.radmeas.2005.11.001, 2006.